Journal of Materials Chemistry A

Accepted Manuscript

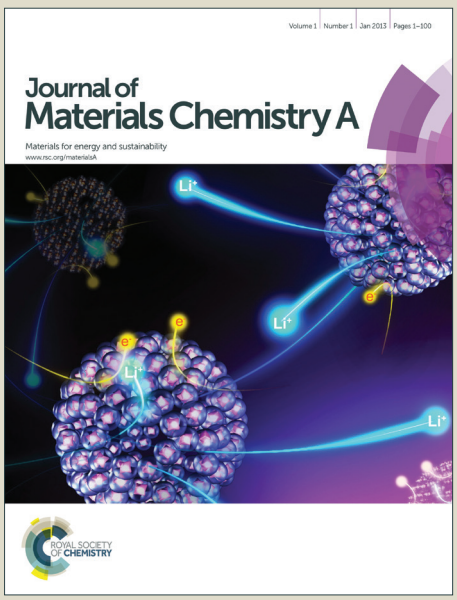

ROYAL SOCIETY OF CHEMISTRY

www.rsc.org/materialsA

Journal Name RSCPublishing

ARTICLE

Co-sensitization of benzoxadiazole based D-A-π-A featured sensitizers: compensating light-harvesting and retarding charge recombination

Cite this: DOI: 10.1039/x0xx00000x

Received 00th January 2012,
Accepted 00th January 2012

DOI: 10.1039/x0xx00000x

www.rsc.org/

Hui Li,[a] Yongzhen Wu,[a] Zhiyuan Geng,*[b] Jingchuan Liu,[a] Dandan Xu,[a] and Weihong Zhu*[a]

Triphenylamine (TPA) dyes usually show relatively narrow spectral response range with respect to indoline and porphyrin based dyes. To optimize light-harvesting, **WS62** and **WS64** are molecularly engineered on basis of D-A-π-A model. We employ TPA in absence or presence of long alkoxy-chain as the electron donor, benzoxadiazole as the auxiliary acceptor, a 4*H*-cyclopenta[1,2-*b*;5,4-*b*']dithiophene (CPDT) unit as the π-bridge, and cyanoacetic acid as the anchor group. The incorporated electron-withdrawing unit of benzoxadiazole enhances the light harvesting by decreasing the molecular energy gap and red-shifting absorption spectra. Moreover, three D-π-A-featured dyes (**S0**, **S1** and **S2**) with different length of π-bridge are developed as co-sensitizers for **WS62** and **WS64**. As demonstrated, the co-sensitization effect is critically dependent upon the π-conjunction length in the three co-adsorbent dyes. Dye **S2** containing dithiophene unit as π-bridge shows a promising co-sensitization result in enhancing photovoltaic efficiency. In contrast, **S1** and **S0** with less thiophene units make a negative contribution to photovoltaic performances. The cocktail co-sensitization of **WS62** and **WS64** with **S2** can compensate the peak valley of IPCE adsorbed by electrolyte near 400 nm and compact the surface of TiO_2 to retard charge recombination, essentially for the optimization of photovoltaic performances. The solar cells based on co-sensitization of **WS64** and **S2** show a high efficiency of 7.9% (V_{OC} of 738 mV, J_{SC} of 14.9 mA cm^{-2} and *FF* of 0.72), exhibiting a significant improvement by 41% compared to the **WS64** alone sensitized devices under the same condition. The charge transfer resistance (R_{CT}) for the co-sensitized DSSCs is larger than that of DSSC comprising only **WS62** or **WS64** by around 10-fold, indicating that the unfavourable charge transfer from TiO_2 to electrolyte is efficiently blocked by the cocktail co-sensitization of **S2**. These findings pave a way how to choose the proper and matchable co-sensitizers for further increasing photovoltaic performances of pure organic sensitizers.

1 Introduction

Dye-sensitized solar cells (DSSCs) are under intensive interdisciplinary investigation in both academia and industry worldwide due to its cost-effective and flexible solar energy conversion.[1,2] Compared with ruthenium (Ru)-based dyes, metal-free organic sensitizers are low-cost and easily modified. However, organic sensitizers show a narrow spectral response range over the broad distribution of sunlight.[3] Multiple dyes used as "dye cocktails"[4] for co-sensitization pave a new approach to panchromatic sensitization[5-7] with preferable photovoltaic performances. An excellent candidate for co-sensitization should compensate the light absorption[4,8] and be moderated for avoiding competitive adsorption. Additionally, the co-sensitization dye should be able to cover the bare TiO_2 surface, prevent the aggregation of dye molecules and retard the charge recombination between TiO_2 and electrolyte.[9-14] As demonstrated, the co-sensitization strategy not only broadens the spectral response range and enhances the light-harvesting,[4] but also retards charge recombination on the surface of TiO_2, thus making an distinct contribution to improve the short-circuit current density (J_{SC}) and open-circuit voltage (V_{OC}).[9]

Recently, D-A-π-A organic sensitizers with incorporation of auxiliary accepters has intensively been explored, resulting in efficient modulation in energy levels, light response as well as a great increase in photo-stability.[15-18] In this work, we developed a couple of new benzoxadiazole based D-A-π-A organic sensitizers **WS62** and **WS64** (Scheme 1), and demonstrated the influence of co-sensitization for improving their photovoltaic performances. Three D-π-A-featured dyes, **S0**, **S1** and **S2** (Scheme 1) containing different number of thiophene units were also developed as

co-sensitizers for **WS62** and **WS64**. Interestingly, the co-sensitization effect is critically dependent upon the π-conjunction length of the three co-sensitizers. Compared with **WS64** alone, the co-sensitization of **WS64** with **S2** is optimized, resulting in a significant improve by 41% in photovoltaic efficiency.

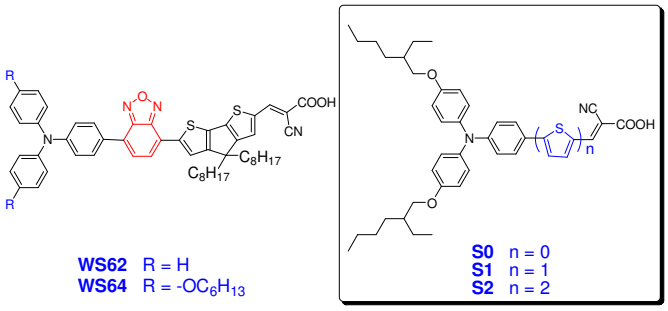

Scheme 1 Chemical structures of sensitizers **WS62**, **WS64**, and co-adsorbents **S0**, **S1** and **S2**.

2 Experimental

2.1 Characterization

^{1}H and ^{13}C NMR spectra were recorded on Brucker AM-400 MHz with tetramethylsilane (TMS) as internal standard. High-resolution mass spectra (HRMS) were performed by using a waters LCT Premier XE spectrometer. The absorption spectra of sensitizer dyes in solution and adsorbed on titania films were measured with a Varian Cary 500 spectrophotometer. The cyclic voltammograms (CV) were obtained with a Versastat II electrochemical workstation (Princeton Applied Research) by using a three-electrode cell with a Pt working electrode, a Pt wire auxiliary electrode, and a saturated calomel reference electrode (SCE) in saturated KCl solution, 0.1 M tetrabutylammonium hexafluorophosphate ($TBAPF_6$) was used as the supporting electrolyte in DCM. Ferrocene was added to each sample solution at the end of the experiments, and the ferrocenium/ferrocene (Fc/Fc^+) redox couple was used as an internal potential reference. Unless otherwise stated, all the raw materials were commercially available from chemical reagent companies, and used without any further purification.

2.2 Synthesis

Synthesis of WS62. A mixture of **1a** (300 mg, 0.38 mmol) and cyanoacetic acid (48 mg, 0.57 mmol) was stirred and heated to reflux for 8 h under argon atmosphere by piperidine (0.4 mL) presented in dry acetonitrile (30 mL). After cooling to room temperature, the crude product was diluted with dichloromethane (DCM, 60 mL), washed with water, dried over anhydrous sodium sulfate, and evaporated the solvent under reduced pressure. The residue was purified by column chromatography with a mixture solution of DCM and methanol (v/v = 10/1) to yield the product **WS62** as powder (261 mg, 0.3 mmol, yield 77%). ^{1}H NMR (400 MHz, DMSO-d_6, ppm): δ 8.28 (s, 1H, alkene-H), 8.12 (s, 1H, dithiophene-H), 8.00 (d, J = 8.6 Hz, 2H, Ph-H), 7.94 (d, J = 7.5 Hz, 1H, benzoxadizaole-H), 7.83 (s, 1H, dithiophene-H), 7.82 (d, J = 7.2 Hz, 1H, benzoxadizaole-H), 7.37 (m, J = 7.7 Hz, 4H, Ph-H), 7.16-7.06 (m, 8H, Ph-H), 1.10-0.93 (m, 28H), 0.74 (t, J = 6.5 Hz, 6H, CH_3). ^{13}C NMR (100 MHz, DMSO-d_6, ppm): δ 155.79, 149.47, 148.37, 147.55, 141.68, 138.98, 129.04, 127.85, 127.39, 126.99, 124.90, 118.67, 117.88, 115.52, 67.59, 30.99, 28.67, 25.19, 22.07, 13.90. HRMS (EIS-MS, *m/z*): $[M - H]^-$ calcd for $C_{53}H_{54}N_4O_3S_2$, 857.3559; found: 857.3557.

Synthesis of WS64. A mixture of **1b** (156 mg, 0.16 mmol) and cyanoacetic acid (20.4 mg, 0.24 mmol) was stirred and heated to reflux for 8 h under argon atmosphere by piperidine (0.4 mL) presented in acetonitrile (20 mL). After cooling to room temperature, the crude product was diluted with DCM (60 mL), washed with water, dried over anhydrous sodium sulfate, and evaporated the solvent under reduced pressure. The residue was purified by column chromatography with a mixture solution of DCM and methanol (v/v = 10/1) to yield the product **WS64** as powder (113 mg, 0.11 mmol, yield 70%). ^{1}H NMR (400 MHz, THF-d_8, ppm): δ 8.28 (s, 1H, alkene-H), 8.05 (s, 1H, dithiophene-H), 7.86 (d, J = 7.0 Hz, 2H, benzoxadizaole-H), 7.69 (d, J = 8.5 Hz, 2H, Ph-H), 7.58 (s, 1H, dithiophene-H), 6.99 (d, J = 8.5 Hz, 4H, Ph-H), 6.86 (d, J = 8.5 Hz, 2H, Ph-H), 6.78 (d, J = 8.5 Hz, 4H, Ph-H), 3.85 (t, J = 6.0 Hz, 4H), 1.30-1.10 (m, 44H), 0.81 (t, J = 6.5 Hz, 6H, CH_3). ^{13}C NMR (100 MHz, THF-d_8, ppm): δ 170.58, 155.95, 139.42, 128.34, 126.70, 118.48, 114.73, 67.38, 53.75, 37.15, 31.36, 31.20, 29.50, 29.24, 28.90, 28.81, 25.37, 22.15, 22.07, 18.96, 13.00. HRMS (EIS-MS, *m/z*): $[M - H]^-$ calcd for $C_{65}H_{78}N_4O_5S_2$, 1057.5335; found: 1057.5334.

Synthesis of S1. A mixture of **2c** (403 mg, 0.66 mmol) and cyanoacetic acid (84 mg, 1.00 mmol) was stirred and heated to reflux for 8 h under argon atmosphere by piperidine (0.4 mL) presented in dry acetonitrile (30 mL). After cooling to room temperature, the crude product was diluted with DCM, washed with water, dried over anhydrous sodium sulfate, and evaporated the solvent under reducing pressure. The residue was purified by column chromatography with a mixture solution of DCM and methanol (v/v = 10/1) to yield the product **S1** as red powder (339 mg, 0.5 mmol, yield 76%). ^{1}H NMR (400 MHz, DMSO-d_6, ppm): δ 8.11 (s, 1H, alkene-H), 7.68 (d, J = 4.0 Hz, 1H, thienyl-H), 7.51 (d, J = 8.7 Hz, 2H, Ph-H), 7.43 (d, J = 3.8 Hz, 1H, thienyl-H), 7.05 (d, J = 8.8 Hz, 4H, Ph-H), 6.93 (d, J = 8.9 Hz, 4H, Ph-H), 6.77 (d, J = 8.8 Hz, 2H, Ph-H), 3.83 (d, J = 5.6 Hz, 4H, OCH_2), 1.67 (t, J = 1.7 Hz, 2H, C*H*CH_2), 1.24-1.64 (m, 18H), 0.88-0.92 (m, 12H, CH_3). ^{13}C NMR (100 MHz, DMSO-d_6, ppm): δ 163.81, 155.83, 149.02, 139.16, 136.95, 134.42, 127.16, 126.79, 123.88, 122.68, 119.05, 118.52, 116.83, 115.52, 115.31, 70.03, 29.90, 28.42, 23.27, 22.50, 13.94, 10.90. HRMS (EIS-MS, *m/z*): $[M - H]^-$ calcd for $C_{43}H_{51}NO_4S$: 677.3413; found: 677.3414.

Synthesis of S2. A mixture of **2d** (541 mg, 0.78 mmol) and cyanoacetic acid (99 mg, 1.17 mmol) was stirred and heated to reflux for 8 h under argon atmosphere by piperidine presented in dry acetonitrile (35 mL). After cooling to room temperature, the crude product was diluted with DCM, washed with water, dried over anhydrous sodium sulfate, and evaporated the solvent under

reducing pressure. The residue was purified by column chromatography with a mixture solution of DCM and methanol (v/v = 10/1) to yield the product **S2** as red powder (464 mg, 0.61 mmol, yield 78%). ^{1}H NMR (400 MHz, DMSO-d_6, ppm): δ 8.07 (s, 1H, alkene-H), 7.66 (d, J = 4.0 Hz, 1H, thienyl-H), 7.51 (d, J = 8.7 Hz, 2H, thienyl-H), 7.46 (d, J = 3.8 Hz, 1H, thienyl-H); 7.43 (d, J = 3.8 Hz, 1H, thienyl-H); 7.36 (d, J = 3.8 Hz, 1H, Ph-H), 7.04 (d, J = 8.9 Hz, 4H, Ph-H), 6.93 (d, J = 8.9 Hz, 4H, Ph-H), 6.76 (d, J = 8.8 Hz, 2H), 3.83 (d, J = 5.6 Hz, 4H, OCH_2), 1.67 (t, J = 1.7 Hz, 2H, C*H*CH_2), 1.24-1.64 (m, 18H), 0.88-0.92 (m, 12H, CH_3). ^{13}C NMR (100 MHz, THF-d_8, ppm): δ 156.09, 148.77, 145.56, 140.25, 135.06, 133.87, 126.65, 126.06, 125.46, 123.38, 122.58, 119.88, 115.05, 70.11, 39.66, 30.57, 29.10, 23.00, 13.48, 10.55. HRMS (EIS-MS, *m/z*): $[M - H]^-$ calcd for $C_{47}H_{53}NO_4S_2$: 759.3290; found: 759.3290.

Synthesis of S0. S0 was obtained as a red powder (481 mg, 0.81 mmol, yield 80%) in a similar way as **S1** and **S2**. ^{1}H NMR (400 MHz, DMSO-d_6, ppm) δ: 7.89 (s, 1H, alkene-H), 7.73 (d, J = 8.5 Hz, 2H, Ph-H), 7.12 (d, J = 8.6 Hz, 4H, Ph-H), 6.96 (d, J = 8.7 Hz, 4H, Ph-H), 6.69 (d, J = 8.5 Hz, 2H, Ph-H), 3.84 (d, J = 5.4 Hz, 4H, OCH_2), 1.67 (t, J = 1.7 Hz, 2H, C*H*CH_2), 1.24-1.64 (m, 18H), 0.88-0.92 (m, 12H, CH_3). ^{13}C NMR (100 MHz, DMSO-d_6, ppm): δ = 156.48, 151.19, 138.22, 131.49, 127.93, 122.87, 119.22, 116.33, 115.64, 70.05, 29.89, 28.40, 23.26, 22.49, 13.93, 10.89. HRMS (EIS-MS, *m/z*): $[M - H]^-$ calcd for $C_{39}H_{49}NO_4$: 595.3536; found: 595.3536.

2.3 Fabrication of nanocrystalline TiO_2 solar cells

Double layer TiO_2 films, Pt-counter electrodes and devices were fabricated according to our published procedures.[25] A double-layer TiO_2 film was composed of a 12 μm thickness nanoporous TiO_2 layer and a 5 μm thickness scattering layer 0.12 cm^2. The TiO_2 films were immersed into the dye solution (4 mM in a mixture of $CHCl_3$:CH_3OH = 4:1) of **WS62** and **WS64** for 12 h, respectively. After that, the sensitized electrodes were rinsed with dry CH_2Cl_2 and dried, and then they were immersed into **S1**, **S2** and **S0** dye solutions (4 mM in a mixture of $CHCl_3$:CH_3OH= 4:1) for half hour. If immersed too long time, the competitive adsorption became serious, especially in the solution of **S0**. Electrolyte was composed of 0.5 M 1-butyl-3-methy imidazolium, 0.5 M 4-*tert*-butylpyridine, 0.1 M lithium iodide and 0.03 M I_2 in the mixed solution of acetonitrile and valeronitrile (v/v = 85/15).

2.4 Photovoltaic performance measurements

The counter electrode (Pt-coated TCO) and the working electrode (dye-loaded TiO_2 film) were sealed together by a hot-melt 30 μm-thick spacer (Surlyn, from Solaronix, Switzerland) under heat pressure. The DSSCs were evaluated by recording the J–V curves with a Keithley 2400 source meter under the illumination of Air Mass 1.5G simulated solar light coming from a solar simulator (Oriel-91160 equipped with a 500 W xenon lamp and an AM 1.5 filter), with a wavelength sampling interval of 10 nm. Incident monochromatic IPCE spectra were measured by an Oriel-66902 system (Oriel Instruments). The incident light intensity was calibrated with a standard reference silicon solar cell (Oriel-91150) and the intensity of incident monochromatic was measured with a Si detector (Oriel-71640). In this work, 100 mW cm^{-2} simulated AM1.5G light is almost the same as the integrated current density from IPCE spectrum and AM1.5G solar emission spectrum, keeping the measured efficiency reliable.

2.5 Electrochemical impedance spectra (EIS) measurements

EIS experiments were carried out in the dark with a ZAHNER ENNIUM electrochemical workstation, with a frequency range from 50 mHz to 100 kHz and a potential amplitude of 10 mV. The obtained impedance spectra were fitted with the ZSimpWin software (v3.10) in terms of appropriate equivalent circuits.

3 Results and Discussion

3.1 Design and synthesis

In **WS62** and **WS64**, we employed triphenylamine as the electron donor, 4*H*-cyclopenta[1,2-*b*;5,4-*b'*]dithiophene (CPDT) as the π-bridge, benzoxadiazole as the auxiliary electron-withdrawing unit, and cyanoacetic acid as the anchor/acceptor (Scheme 1). The difference between **WS62** and **WS64** is the absence or presence of alkoxy chains. Incorporating the auxiliary electron-withdrawing unit of benzoxadiazole is expected to optimize the molecule HOMO-LUMO energy gap and facilitate the intramolecular charge transfer from the donor to the anchor.[18] Instead of the traditional thiophene unit as π-bridge, CPDT unit can increase the conjugation degree for further narrowing the HOMO-LUMO band gap and enhancing the intramolecular charge transfer process. In addition, the long alkyl chain (octyl group) substituted on CPDT unit is beneficial to suppress the dye aggregation behaviour.[19-21] Since dendritic molecules are beneficial to forming a dense monolayer and effectively blocking charge recombination,[11,22] three co-sensitizers (**S0**, **S1** and **S2**) were developed with alkoxy-chain-decorated triphenylamine donor by the different length of π-bridge. The synthetic routes of these dyes are depicted in Scheme 2. Suzuki coupling reaction and Knoevenagel condensation were mainly used for synthesizing the targeted structures that were characterized by ^{1}H, ^{13}C NMR, and HRMS (Experimental Section).

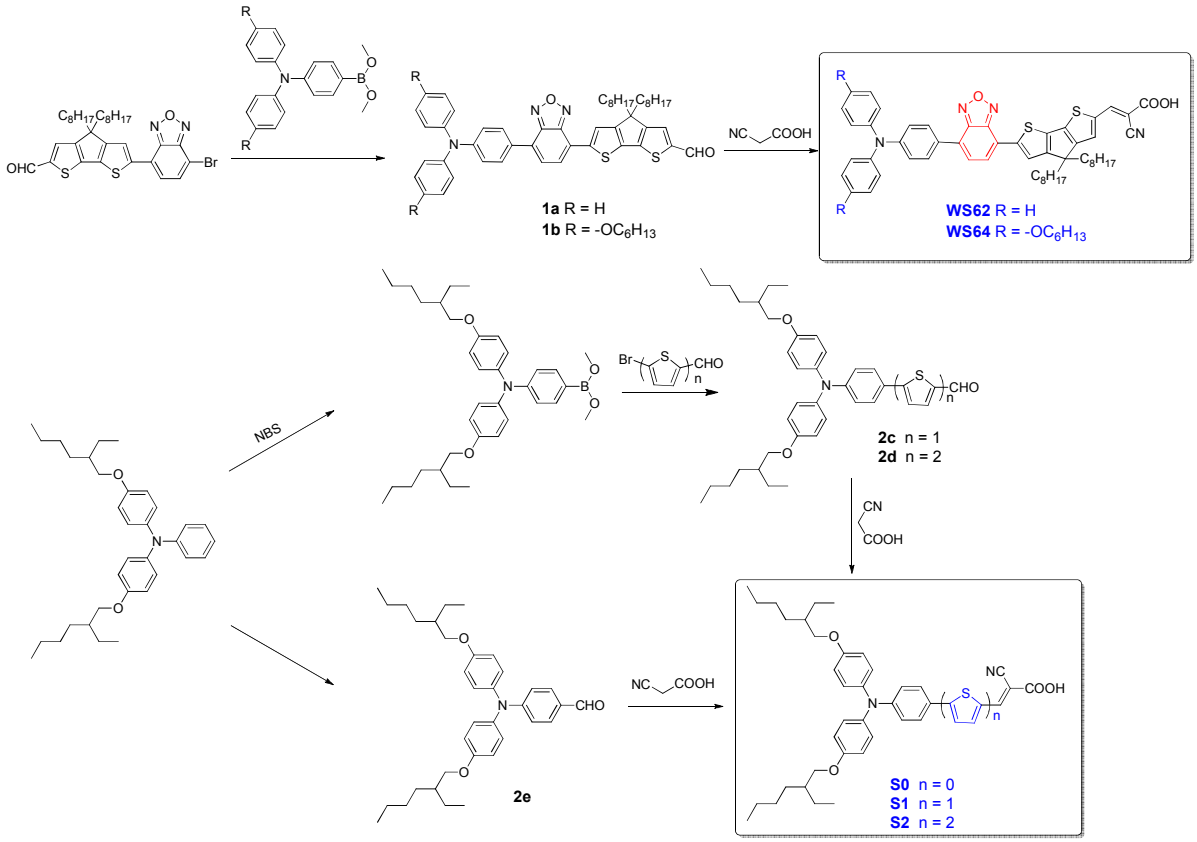

Scheme 2 Synthetic routes to **WS62**, **WS64**, **S0**, **S1** and **S2**.

3.2 Optical properties

The UV-Vis absorption spectra of **WS62** and **WS64** were determined in dilute CH_3OH and $CHCl_3$ mixed solution (v/v = 1:4, Fig. 1a). They show similar absorption curves with three absorption bands at around 300, 450 and 550 nm (Table 1), which is in consistent with our previous results.[16,17,23-25] The band located at 301 nm is due to the localized $\pi \rightarrow \pi^*$ transitions. The intramolecular charge transfer absorption peaks in the visible region are located at 543 and 559 nm for **WS62** and **WS64**, respectively. Obviously, the introduction of alkoxy chains on TPA donor can red-shift the absorption band by 16 nm,[26-30] and enhance the molar absorption coefficient from 3.99×10^4 to 4.70×10^4 M^{-1} cm^{-1}. Besides, a third (shoulder) absorption band is observed at 454 and 464 nm for **WS62** and **WS64**, respectively. Obviously, there is a deep valley at around 400 nm in the absorption curves of both **WS62** and **WS64**, which may cause low IPCE response at this region, especially considering the strong light absorption by the triiodide (I_3^-) in the electrolyte. Therefore, co-sensitization with compensating light-harvesting may benefit to the device performance of both **WS62** and **WS64**. The absorption spectra of dyes **S0**, **S1** and **S2** were shown in Fig. 1b. Upon changing the thiophene number from zero to 1 and 2, the absorption bands for **S0**, **S1** and **S2** are gradually red-shifted with band peaks located at 418, 465 and 478 nm (Table 1), respectively. The strong absorption of these dyes at short wavelength region make them attractive for co-sensitization with **WS62** and **WS64**.

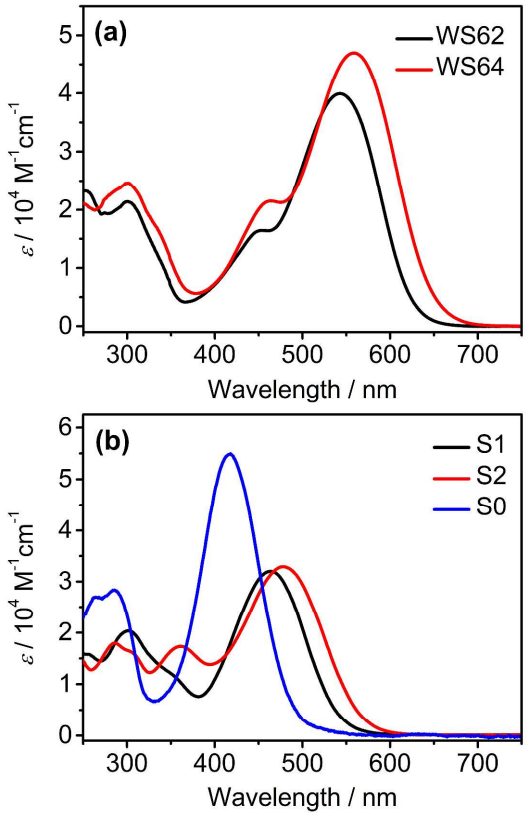

Fig. 1 UV-visible absorption spectra in the mixed solution of CH_3OH and $CHCl_3$ (v/v = 1:4): (a) **WS62** and **WS64**, (b) co-sensitizers **S0**, **S1** and **S2.**

Table 1 Photophysical and electrochemical properties of dyes **S0**, **S1**, **S2**, **WS62** and **WS64**.

Dyes	λ_{max} in solution [nm][a]	ε [M^{-1} cm^{-1}][a]	λ_{max} on TiO_2 [nm][b]	HOMO [V][c]	$E_{0\text{-}0}$ [V][d]	LUMO [V][d]
S0	418	55000	417	0.85	2.38	-1.53
S1	465	32000	458	0.99	2.15	-1.16
S2	478	32900	465	1.02	2.06	-1.04
WS62	301	21400	517	1.09	1.93	-0.84
	454	16400				
	543	39900				
WS64	301	24700	533	0.84	1.84	-1.00
	464	21500				
	559	47000				

[a]bsorption peaks (λ_{max}) and molar extinction coefficients (ε) in the mixed solution of CH_3OH and $CHCl_3$ (v/v = 1 : 4); [b]bsorption peaks on TiO_2 films; [c]HOMO measured in methylene chloride with cyclic voltammograms (CV) at the scan rate of 100 mV/s. [d]$E_{0\text{-}0}$ estimated from the absorption thresholds in absorption spectra of dyes adsorbed on TiO_2 film, LUMO estimated by subtracting $E_{0\text{-}0}$ from the HOMO.

3.3 Photovoltaic device performances

Firstly, we studied the individual dye sensitized devices. Dyes **WS62**, **WS64**, **S1**, **S2** and **S0** based devices are denoted as A1, B1, C, D and E, respectively. Their photovoltaic parameters were collected in Table 2. All of these dyes showed moderate power conversion efficiency of 4.4-6.3% under AM 1.5 simulated sun light. Although the two D-A-π-A dyes shows broad light absorption range, their performances in DSSCs is not as high as reported benzothiadiazole and quinoxaline based sensitizers.[16-18] Devices based on **WS62** and **WS64** (A1 and B1) only gave efficiency of 4.4% (V_{OC} of 615 mV, J_{SC} of 9.9 mA cm^{-2}, *FF* of 0.73) and 5.6% (V_{OC} of 668 mV, J_{SC} of 11.7 mA·cm^{-2}, *FF* of 0.71), respectively. Their *J-V* curves were shown in Fig. 2. According to the HOMO and LUMO energy levels of both dyes in Table 1, we can rule out the mismatch possibility in energy level since the driving forces for the efficient electron injection and dye regeneration of **WS62** and **WS64** are thermodynamically favorable. We speculated that the CPDT unit with a relatively large and planar structure made dyes easy to aggregate. Even though incorporating two long alkyl chains on the CPDT unit,[31-33] it is still not enough to suppress aggregation efficiently. On the other hand, the IPCE curves of **WS62** and **WS64** (Fig. 3) showed a significant valley at around 400 nm, which might be resulted from the combination of low absorbance of the dyes and competitive absorption of triiodide in the electrolyte. Therefore, we studied the effect of co-sensitization with **S0**, **S1** and **S2**.

The devices based on co-sensitization of **WS62** with **S1**, **S2** and **S0** are coded as A2, A3 and A4, respectively. Similarly, devices based on co-sensitization of **WS64** with **S1**, **S2** and **S0** are coded as B2, B3 and B4. The photoanode TiO_2 films were firstly immersed into the dye solution (4 mM in a mixture of $CHCl_3$:CH_3OH = 4:1) of **WS62** and **WS64** for 12 h, respectively. Then then they were immersed into **S1**, **S2** and **S0** dye solutions (4 mM in a mixture of $CHCl_3$:CH_3OH= 4:1) for half hour. Interestingly, a significant influence on the performance of co-sensitized devices was observed. As the number of thiophene unit increased, the efficiency of co-sensitized device increased significantly. Encouragingly, devices of **A3** and **B3** based on co-sensitization of **WS62** and **WS64** with **S2** produced photovoltaic efficiency of 6.5% (**WS62+S2**, device A3) and 7.9% (**WS64+S2**, Device B3), which were significantly improved by 48% and 41% with respect to **WS62** and **WS64** dye alone under the same condition (Table 2). Obviously, co-sensitization with **S2** increased both J_{SC} and V_{OC} to a great extent. In contrast, co-sensitization with **S1** and **S0** resulted in much less improvement in the photovoltaic efficiency. Therefore, the delicate molecular structure plays an important role in the co-sensitization process, which is discussed in the following theoretical studies.

Table 2 Photovoltaic parameters of DSSCs based on **WS62** and **WS64** with/without co-sensitization measured under simulated AM1.5G solar light (100 mW cm^{-2}).

Device	dye	V_{OC} (mV)	J_{SC} (mA cm^{-2})	*FF*	η (%)
A1	**WS62**	615	9.9	0.73	4.4
A2	**WS62+S1**	621	10.9	0.74	5.0
A3	**WS62+S2**	641	14.5	0.70	6.5
A4	**WS62+S0**	623	9.0	0.73	4.1
B1	**WS64**	668	11.7	0.71	5.6
B2	**WS64+S1**	674	12.8	0.72	6.2
B3	**WS64+S2**	738	14.9	0.72	7.9
B4	**WS64+S0**	672	9.8	0.73	4.8
C	**S1**	758	9.2	0.70	4.9
D	**S2**	734	12.3	0.70	6.3
E	**S0**	744	8.4	0.71	4.4

In order to take insight into the co-sensitization improvement of J_{SC} (device A3, **W62+S2**; device B3, **WS64+S2**), their IPCE spectra were carefully compared with individual dye (device A1, **WS62**; device B1, **WS64**). As shown in Fig. 3, the co-sensitizer of **S2** makes a preferable contribution to the IPCE improvement, mostly around 400 nm. Generally, the competitive light absorption by I_3^- in the electrolyte affects the light-harvesting efficiency of dyes in the wavelength range from 350 to 400 nm. However, the co-sensitization with **S2** can recover the IPCE loss caused by I_3^- (Fig. 3). Actually, **S2** has two absorption peaks at 368 and 465 nm (Fig. 1b), which can exactly compensate light absorption in the region for enhancing light harvesting. The IPCE onsets for **WS62**, **WS64**, **WS62+S2**, and **WS64+S2** are 789, 820, 770 and 810 nm, respectively. Notice that the co-sensitization with **S2** can blue shift the IPCE onset of **WS62** and **WS64** to some extent. Although the co-sensitization of **S2** can replace some host dye molecules with narrow IPCE onset, the IPCE platform upon co-sensitization with **S2** become higher, resulting in an overall increase in IPCE and J_{sc}.[35,36] Compared to individual **WS62** and **WS64** based devices, the V_{oc} of co-sensitized cells were also largely improved (Table 2).

Furthermore, we studied the co-sensitized photoanode in the reverse dipping order, that is, the TiO_2 films were firstly immersed in S series dyes for half hour, and then were immersed in WS series

dyes for 12 h. Besides the sequence dipping, the immersion in a mixture of two co-sensitized dyes for 12 h was also tested. Their photovoltaic parameters were less efficient than their corresponding devices (sensitized by WS and S series in proper order, Table 2). For example, compared with device B3, the efficiency of co-sensitized devices in reverse order was decreased to 6.7% (V_{OC} of 664 mV, J_{SC} of 14.2 mA cm^{-2}, *FF* of 0.72), and the mixture co-sensitization was 7.1% (V_{OC} of 683 mV, J_{SC} of 15.8 mA cm^{-2}, *FF* of 0.70) under the same condition.

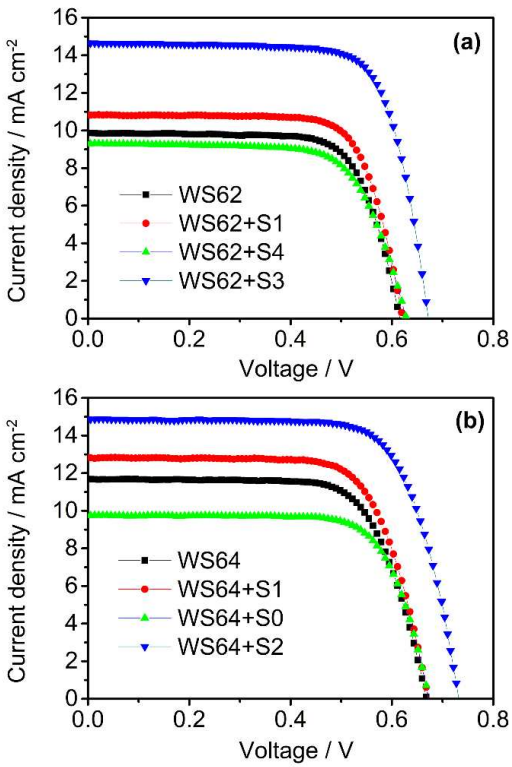

Fig. 2 Photocurrent density-voltage curves of DSSCs based on **WS62** and **WS64** with/without co-sensitization of **S2** under AM 1.5G simulated solar light (100 mW cm^{-2}).

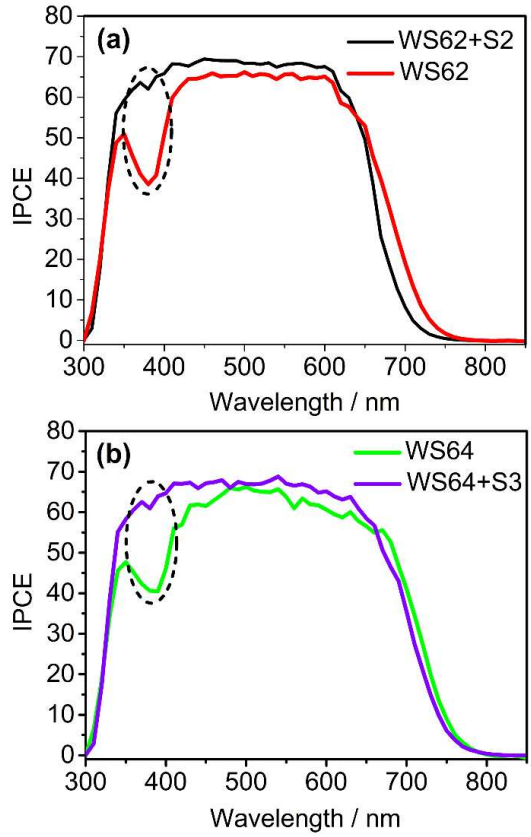

Fig. 3 IPCE spectra of DSSCs based on **WS62** and **WS64** with/without co-sensitization of **S2** under 100 mW cm^{-2} irradiation.

3.4 Electrochemical impedance spectroscopy (EIS)

EIS is a versatile method to study charge recombination at the TiO_2/electrolyte interface, determined under a range of potentials near the V_{OC} values of **WS62**, **WS64**, **WS62+S2**, and **WS64+S2** in the dark. The resulting data were fitted with an equivalent circuit to extract the chemical capacitance (C_μ) and charge transfer resistance (R_{CT}) at the TiO_2/dye/electrolyte interface.[37] As shown in Fig. 4, the logarithms of R_{CT} values were decreased linearly with increasing bias potential. At a fixed bias potential of 0.60 V, the R_{CT} for the co-sensitized DSSC was larger than that of DSSC comprising only **WS62** or **WS64** by around 10-fold, indicating that the unfavourable charge transfer from TiO_2 to electrolyte is efficiently blocked by the cocktail co-sensitization of **S2**.

Generally, V_{OC} is dependent upon the difference between the quasi-Fermi level of TiO_2 and the redox potential of the electrolyte (E_{redox}), which can be illustrated by Equation (1):

$$V_{OC} = \frac{E_{CB}}{q} + \frac{KT}{q}\ln\left(\frac{n}{N_{CB}}\right) - \frac{E_{redox}}{q} \quad (1)$$

Where E_{CB} is the conduction band edge of TiO_2, q the elementary charge, K the Boltzmann constant, T absolute temperature, n the number of electrons in TiO_2, N_{CB} the effective density of states, and E_{redox} redox potential of the electrolyte. Here the last term E_{redox}/q is

determined to redox potential of I^-/I^-_3, a constant in DSSCs with the I^-/I^-_3 redox couple. That is, V_{OC} is dependent upon the first two terms (E_{CB} and the electron concentration in TiO_2). Obviously, the balance of electron density can be shifted by co-adsorbing with **S2**.[38] We can expect that the interspaces between molecules of **WS62** or **WS64** is filled by the co-sensitizer, thus suppressing the charge recombination on the surface of TiO_2 and increasing the injected electron lifetime in TiO_2 conduction band.

The electron lifetime τ_n can be estimated from equation of $\tau_n = C_\mu * R_{CT}$.[37] Fig. 5 shows the electron lifetime as a function of bias potential at open circuit for the DSSCs based on **WS62** and **WS64** with/without co-sensitization. Under a bias potential of 0.6 V, the electron lifetime of **WS64** and **WS64+S2** are 0.0122 and 0.4350 s, respectively. Obviously, the co-sensitization of **WS64** with **S2** increases the electron lifetime by one order of magnitude. Similarly, the co-sensitization of **WS62** with **S2** increases the electron lifetime by two order of magnitude, from 0.0012 s to 0.13 s. The prolonged electron lifetime in co-sensitization is beneficial to the charge accumulation in TiO_2 conduction band under open-circuit, thus increasing the electron density and Fermi level of TiO_2. As well known, the V_{OC} of DSSC is determined by the difference between TiO_2 Fermi level and redox potential of electrolyte. The measured electron lifetime is in agreement with the *V*oc values of these devices (Table 2). Therefore, the cocktail co-sensitization of **S2** with **WS62** and **WS64** can efficiently block the interfacial charge recombination loss and enhances the electron lifetime, which accounts well for the rendering higher V_{OC} in the co-sensitized devices.

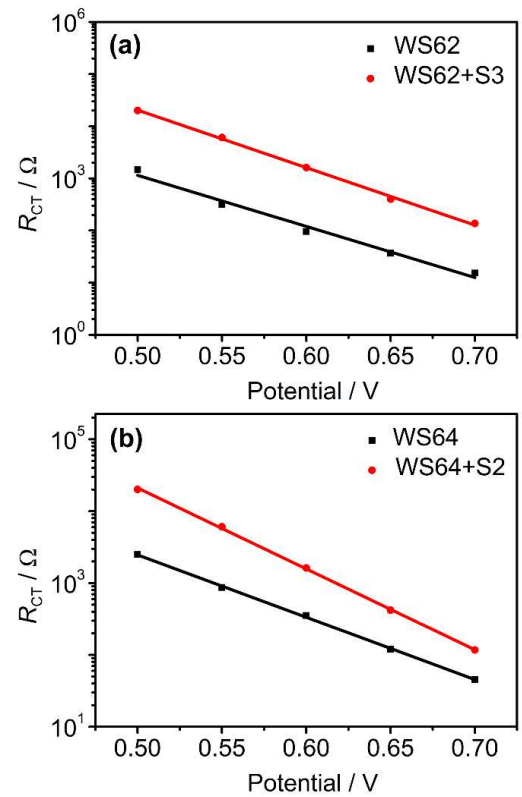

Fig. 4 Interfacial charge transfer resistance (R_{CT}) in TiO_2 of DSSCs based on **WS62** and **WS64** with/without co-sensitization of **S2** in the dark at the difference potentials.

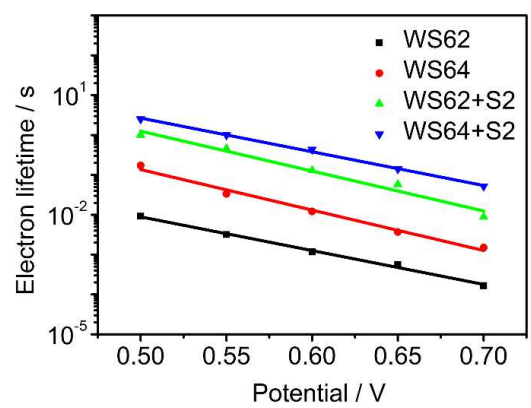

Fig. 5 Electron lifetime (τ_n) spectra of DSSCs based on **WS62** and **WS64** with/without co-sensitization of **S2** fitted from EIS spectra under a series of applied potentials.

Table 3 Calculated HOMO and LUMO profiles and energy levels of **WS62**, **WS64**, **S0**, **S1** and **S2** (orbital energies are in eV).

	WS62	WS64	S0	S1	S2
HOMO	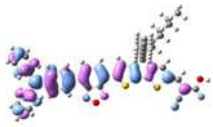 -5.07	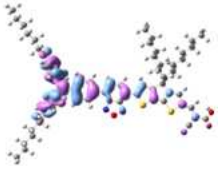 -4.85	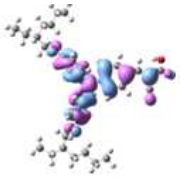 -5.26	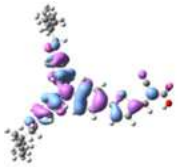 -4.99	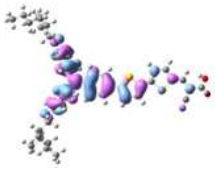 -4.87
LUMO	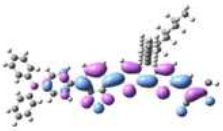 -2.96	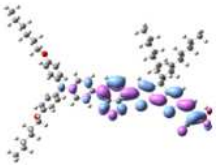 -2.93	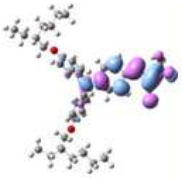 -2.22	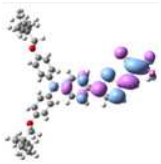 -2.55	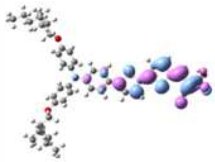 -2.71

3.5 Theoretical approach

TD-DFT calculations performed with Gaussian 09 program package at the B3LYP/6-31G* (LANL2DZ for Ti atom) level[39] were employed in further exploring the dependence of charge recombination on the molecular geometries and orbitals. Table 3 shows the frontier molecular orbital profiles, and optimized molecular structures with the calculated HOMO and LUMO levels for sensitizers and co-adsorbents. In case of **WS62** and **WS64**, the electron density is predominately distributed along the D-A system (TPA and benzoxadiazole) at HOMO orbital; while at the LUMO orbital, electrons are transferred intramolecularly and delocalized across the entire A-π-A system. Here electrons can successively transfer from the donor (TPA) to benzoxadiazole, then transfer to the anchor (cyanoacetic acid) and finally to TiO_2.[40] The additional alkoxy-chains on **WS64** also upshifts the HOMO but barely influences the LUMO. In case of co-sensitization dyes (**S1**, **S2** and **S0**), fusion of thiophene unit can upshift the HOMO and lower the LUMO .

Notably, the bond angles of the double long alkyl chains attached on CPDT unit are 162º, 163º for **WS62** and **WS64**, respectively, under the optimized configuration when adsorbed on the TiO_2 film. Both the large bond angles and long alkoxy chains are expected to extend intermolecular distance, and the electrolyte permeates through TiO_2 surface, thus causing serious charge recombination. Besides, the alkoxy-chains may block co-adsorbents anchoring on TiO_2 films. Consequently, a suitable molecular size is critically important to co-adsorbents.

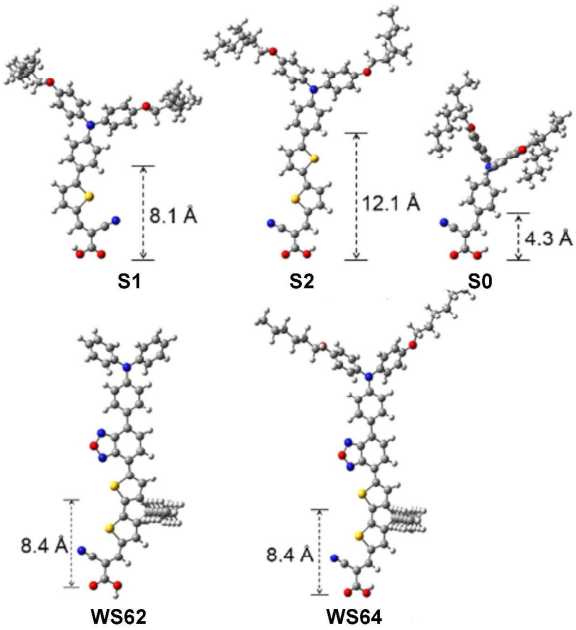

Fig. 6 Optimized molecular structures of **S0**, **S1**, **S2**, **WS62**, and **WS64** calculated from density functional theory.

From theoretical calculations (as shown in Fig. 6), the distance from the TiO_2 films to alkoxy chains in **WS62** and **WS64** is 8.4 Å, and the conjugated length for **S0**, **S1** and **S2** are 4.3, 8.1 and 12.1 Å, respectively. Obviously, the co-adsorbent of **S2** has a relative longer conjugated bridge than **S1** and **S0**, thus ensuring that **S2** has opportunity to overcome the barrier of alkoxy chain and anchor on the TiO_2 film. Besides the dendritic alkoxy-chains, the co-sensitization of **S2** with proper conjugation bridge can guarantee further forming a compact sensitized layer, and preventing I_3^- from approaching to TiO_2 film (Fig. 7). Meanwhile, **S1** and **S0** with the shorter length may have less possibility to go through the barrier when dipped in corresponding dye bath.

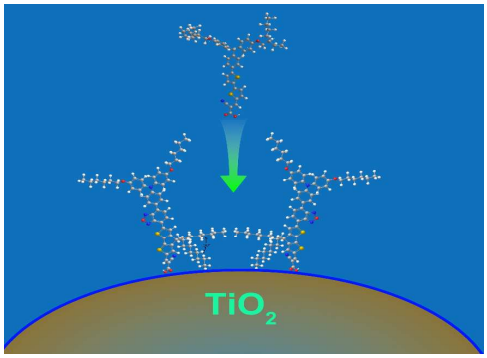

Fig. 7 Schematic dirgram co-sensitization of **WS64** with **S2**.

4 Conclusions

We apply the co-sensitization strategy for benzoxadizaole based D-A-π-A featured metal-free dyes (**WS62** and **WS64**), especially focused on compensating light-harvesting and retarding charge recombination. As found, J_{SC} of co-sensitized solar cell devices is heavily dependent upon the chemical structure of co-absorbents. As a proper π-conjunction size, co-sensitizer dye **S2** containing dithiophene unit can efficiently permeate into the benzoxadizaole based D-A-π-A dye molecules, resulting in a compact co-sensitization layer. Co-sensitization with **S2** can not only compensate the peak valley of IPCE near 400 nm, but also realize the retard charge recombination. Indeed, the increase in J_{SC} is predominated. The photovoltaic efficiencies of **WS62** and **WS64** are improved by 48% and 41%, increased from 4.4% and 5.6% to 6.5% and 7.9%, respectively. This work takes insight how to choose the proper and matchable co-sensitizers for further increasing photovoltaic performances of pure organic sensitizers.

Notes and references

[a]*Shanghai Key Laboratory of Functional Materials Chemistry, Key Laboratory for Advanced Materials and Institute of Fine Chemicals, East China University of Science and Technology, Shanghai 200237, P. R. China; E-mail: whzhu@ecust.edu.cn*
[b]*Gansu Key Laboratory Of Polymer Materials, College of Chemistry and Chemical Engineering, Key Laboratory of Eco-Environment-Related Polymer Materials, Ministry of Edccation, Northwest Normal University, Lanzhou, 730070 Gansu, P. R. China; E-mail: zhiyuangeng@126.com*

1. A. Hagfeldt, G. Boschloo, L. C. Sun, L. Kloo and H. Pettersson, *Chem. Rev.*, 2010, **110**, 6595–6663.
2. B. O'Regan and M. Grätzel, *Nature*, 1991, **353**, 737–740.
3. (*a*) J.-H. Yum, E. Baranoff, S. Wenger, M. K. Nazeeruddin and M. Grätzel, *Energy Environ. Sci.*, 2011, **4**, 842–857; (*b*) J. B. Yang, P. Ganesan, J. Teuscher, T. Moehl, Y. J. Kim, C. Y. Yi, P. Comte, K. Pei, T. W. Holcombe, M. K. Nazeeruddin, J. L. Hua, S. M. Zakeeruddin, H. Tian, and M. Grätzel, *J. Am. Chem. Soc.*, **136**, 5722–5730.
4. (*a*) S. Zhang, A. Islam, X. Yang, C. Qin, K. Zhang, Y. Numata, H. Chen and L. Han, *J. Mater. Chem. A*, 2013, **1**, 4812–4819; (*b*) S. Mathew, A. Yella, P. Gao, R. Humphry-Baker, B. F. E. Curchod, N. Ashari-Astani, I. Tavernelli, U. Rothlisberger, M. K. Nazeeruddin and M. Grätzel, *Nature Chem.*, 2014, **6**, 242–247.
5. N. Robertson, *Angew. Chem. Int. Ed.*, 2008, **47**, 1012–1014.
6. J.-J. Cid, J.-H. Yum, S.-R. Jang, M. K. Nazeeruddin, E. Martínez-Ferrero, E. Palomares, J. Ko, M. Grätzel and T. Torres, *Angew. Chem. Int. Ed.*, 2007, **46**, 8358–8362.
7. H. Choi, S. Kim, S. O. Kang, J. Ko, M.-S. Kang, J. N. Clifford, A. Forneli, E. Palomares, M. K. Nazeeruddin and M. Grätzel, *Angew. Chem. Int. Ed.*, 2008, **47**, 8259–8263.
8. L. Han, A. Islam, H. Chen, C. Malapaka, B. Chiranjeevi, S. Zhang, X. Yang and M. Yanagida, *Energy Environ. Sci.*, 2012, **5**, 6057–6060.
9. G. Li, M. Liang, H. Wang, Z. Sun, L. Wang, Z. Wang and S. Xue, *Chem. Mater.*, 2013, **25**, 1713–1722.
10. J. Xu, H. Wu, X. Jia, H. Kafafy and D. Zou, *J. Mater. Chem. A*, 2013, **1**, 14524–14531.
11. Y. S. Kwon, I. Y. Song, J. Lim, S.-H. Park, A. Siva, Y.-C. Park, H. M. Jang and T. Park, *RSC Advances*, 2012, **2**, 3467–3472.
12. Y.-G. Lee, S. Park, W. Cho, T. Son, P. Sudhagar, J. H. Jung, S. Wooh, K. Char and Y. S. Kang, *J. Phys. Chem. C*, 2012, **116**, 6770–6777.
13. J. Lim, Y. S. Kwon and T. Park, *Chem. Commun.*, 2011, **47**, 4147–4149.
14. M. Wang, C. Grätzel, S.-J. Moon, R. Humphry-Baker, N. Rossier-Iten, S. M. Zakeeruddin and M. Grätzel, *Adv. Funct. Mater.*, 2009, **19**, 2163–2172.
15. (*a*) J. Shi, Z. F. Chai, J. Su, J. N. Chen, R. L. Tang, K. Fan, L. L Zhang, H. W. Han, J. G. Qin, T. Y. Peng, Q. Q. Li and Z. Li, *Dyes Pigm.*, 2013, **98**, 405–413; (*b*) S. Chaurasia, W. I. Hung, H. H. Chou, and J. T. Lin, Org. Lett., 2014, dx.doi.org/10.1021/ol501163b; (*c*) W. L. Ding, D. Wang, Z. Y. Geng, X. L. Zhao and Y.-F. Yan, *J. Phys. Chem. C*, 2013, **117**, 17382–17398; (*d*) L. N. Wang, M. Liang, Y. Zhang, F.Y. Cheng, X. D. Wang, Z. Sun and S. Xue, *Dyes Pigm.*, 2014, **101**, 270–279; (*e*) M. Katono, M. Wielopolski, M. Marszalek, T. Bessho, J. E. Moser, R. Humphry-Baker, S. M. Zakeeruddin and M. Grätzel, *J. Phys. Chem. C*, 2014, dx.doi.org/10.1021/jp411504p.
16. (*a*) Y. Z. Wu and W. H. Zhu, *Chem. Soc. Rev.*, 2013, **42**, 2039–2058; (*b*) K. Pei, Y. Z. Wu, A. Islam, Q. Zhang, L. Y. Han, H. Tian and W. H. Zhu, *ACS Appl. Mater. Interfaces*, 2013, **5**, 4986–4995; (*c*) H. B. Zhu, W. Q. Li, Y. Z. Wu, B. Liu, S. Q. Zhu, X. Li, H. Ågren and W. H. Zhu, *ACS Sustainable Chem. Eng.*, 2014, **2**, 1026–1034.
17. Y. Z. Wu, M. Marszalek, S. M. Zakeeruddin, Q. Zhang, H. Tian, M. Grätzel and W. H. Zhu, *Energy Environ. Sci.*, 2012, **5**, 8261–8272.
18. W. H. Zhu, Y. Z. Wu, S. T. Wang, W. Q. Li, X. Li, J. Chen, Z.-S. Wang and H. Tian, *Adv. Funct. Mater.*, 2011, **21**, 756–763.
19. M. Horie, J. Kettle, C.-Y. Yu, L. A. Majewski, S.-W. Chang, J. Kirkpatrick, S. M. Tuladhar, J. Nelson, B. R. Saunders and M. L. Turner, *J. Mater. Chem.*, 2012, **22**, 381–389.
20. L. Ying, B. B. Y. Hsu, H. Zhan, G. C. Welch, P. Zalar, L. A. Perez, E. J. Kramer, T.-Q. Nguyen, A. J. Heeger, W.-Y. Wong and G. C. Bazan, *J. Am. Chem. Soc.*, 2011, **133**, 18538–18541.
21. M. Zhang, J. Zhang, Y. Fan, L. Yang, Y. Wang, R. Li and P. Wang, *Energy Environ. Sci.*, 2013, **6**, 2939–2943.
22. J. Xu, H. Wu, X. Jia and D. Zou, *Chem. Commun.*, 2012, **48**, 7793–7795.
23. W. Q. Li, Y. Z. Wu, Q. Zhang, H. Tian and W. H. Zhu, *ACS Appl. Mater. Interfaces*, 2012, **4**, 1822–1830.
24. Y. Cui, Z. Y. Wu, X. F. Lu, X. Zhang, G. Zhou, F. B. Miapeh, W. H. Zhu and Z.-S. Wang, *Chem. Mater.*, 2011, **23**, 4394–4401.
25. K. Pei, Y. Z. Wu, W. J. Wu, Q. Zhang, B. Q. Chen, H. Tian and W. H. Zhu, *Chem. Eur. J.*, 2012, **18**, 8190–8200.
26. C. Teng, X. Yang, C. Yang, S. Li, M. Cheng, A. Hagfeldt and L. Sun, *J. Phys. Chem. C*, 2010, **114**, 9101–9110.
27. Y. Numata, I. Ashraful, Y. Shirai and L. Han, *Chem. Commun.*, 2011, 47, 6159–6161.
28. B. Liu, Q. Liu, D. You, X. Li, Y. Naruta and W. Zhu, *J. Mater. Chem.*, 2012, **22**, 13348–13356.
29. D. P. Hagberg, J.-H. Yum, H. Lee, F. De Angelis, T. Marinado, K. M. Karlsson, R. Humphry-Baker, L. Sun, A. Hagfeldt, M. Grätzel and M. K. Nazeeruddin, *J. Am. Chem. Soc.*, 2008, **130**, 6259–6266.
30. A. Mishra, M. K. R. Fischer and P. Bäuerle, *Angew. Chem. Int. Ed.*, 2009, **48**, 2474–2499.
31. M. Zhang, J. Liu, Y. Wang, D. Zhou and P. Wang, *Chem. Sci.*, 2011, **2**, 1401–1406.
32. T. Marinado, K. Nonomura, J. Nissfolk, M. K. Karlsson, D. P. Hagberg, L. Sun, S. Mori and A. Hagfeldt, *Langmuir*, 2009, **26**, 2592–2598.

33. B. C. O'Regan, K. Walley, M. Juozapavicius, A. Anderson, F. Matar, T. Ghaddar, S. M. Zakeeruddin, C. Klein and J. R. Durrant, *J. Am. Chem. Soc.*, 2009, **131**, 3541–3548.
34. D. Cahen, G. Hodes, M. Grätzel, J. F. Guillemoles and I. Riess, *J. Phys. Chem. B*, 2000, **104**, 2053–2059.
35. P. Wang, S. M. Zakeeruddin, P. Comte, R. Charvet, R. Humphry-Baker and M. Grätzel, *J. Phys. Chem. B*, 2003, **107**, 14336–14341.
36. S. H. Kang, I. T. Choi, M. S. Kang, Y. K. Eom, M. J. Ju, J. Y. Hong, H. S. Kang and H. K. Kim, *J. Mater. Chem. A*, 2013, **1**, 3977–3982.
37. Y. Liang, B. Peng and J. Chen, *J. Phys. Chem. C*, 2010, **114**, 10992–10998.
38. Z. Ning, Y. Fu and H. Tian, *Energy Environ. Sci.*, 2010, **3**, 1170–1181.
39. M. J. Frisch, G. W. Trucks, H. B. Schlegel, P. M. W. Gill, B. G. Johnson, M. A. Robb, J. R. Cheeseman, T. Keith, G. A. Petersson, J. A. Montgomery, K. Raghavachari, M. A. Al-Laham, V. G. Zakrzewski, J. V. Ortiz, J. B. Foresman, J. Cioslowski, B. B. Stefanov, A. Nanayakkara, M. Challacombe, C. Y. Peng, P. Y. Ayala, W. Chen, M. W. Wong, J. L. Andres, E. S. Replogle, R. Gomperts, R. L. Martin, D. J. Fox, J. S. Binkley, D. J. Defrees, J. Baker, J. P. Stewart, M. Head-Gordon, C. Gonzalez and J. A. Pople, Gaussian 03, revision C.01, Gaussian, Inc., Pittsburgh, PA, 2004.
40. J. Zeng, T. Zhang, X. Zang, D. Kuang, H. Meier and D. Cao, *Sci. China Chem.*, 2013, **56**, 505–513.

Graphics for Contents

Co-sensitization of triphenylamine based D-A-π-A featured sensitizers: compensating light-harvesting and retarding charge recombination

Hui Li,[a] Yongzhen Wu,[a] Zhiyuan Geng,[b] Jingchuan Liu,[a] Dandan Xu,[a] and Weihong Zhu*[a]*

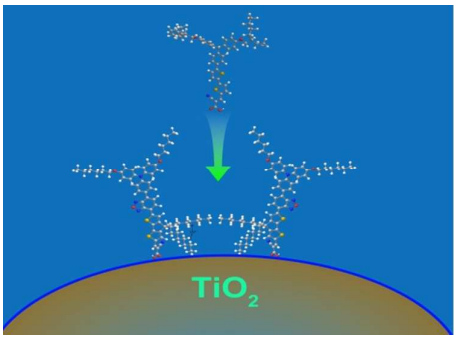

The cocktail co-sensitization of **WS62** and **WS64** with **S2** can compensate the peak valley of IPCE adsorbed by electrolyte near 400 nm and compact the surface of TiO_2 to retard charge recombination, essentially for the optimization of photovoltatic performances.